Towards a Measurement of the Lamb Shift in Muonic Hydrogen

R. Pohl[1,2⋆], F. Biraben[3], C.A.N. Conde[4], C. Donche-Gay[5], T.W. Hänsch[6], F.J. Hartmann[7], P. Hauser[1], V.W. Hughes[8], O. Huot[5], P. Indelicato[3], P. Knowles[5], F. Kottmann[2], Y.-W. Liu[8,1], V.E. Markushin[1], F. Mulhauser[5], F. Nez[3], C. Petitjean[1], P. Rabinowitz[9], J.M.F. dos Santos[4], L.A. Schaller[5], H. Schneuwly[5], W. Schott[7], D. Taqqu[1], and J.F.C.A. Veloso[4]

[1] Paul Scherrer Institute, CH-5232 Villigen PSI, Switzerland
[2] Institut für Teilchenphysik, ETHZ, CH-8093 Zürich, Switzerland
[3] Laboratoire Kastler Brossel, F-75252 Paris CEDEX 05, France
[4] Departamento de Fisica, Universidade de Coimbra, P-3000 Coimbra, Portugal
[5] Institut de Physique de l'Université, CH-1700 Fribourg, Switzerland
[6] Max-Planck-Institut für Quantenoptik, D-85748 Garching, Germany
[7] Physik-Department, Technische Universität München, D-85747 Garching, Germany
[8] Physics Department, Yale University, New Haven, CT06520-8121, USA
[9] Department of Chemistry, Princeton University, Princeton, NJ08544-1009, USA

Abstract. The availability of long-lived metastable muonic hydrogen atoms (μp) in the 2S state has been investigated in a recent series of experiments at PSI. From the low-energy part of the initial kinetic energy distribution of μp(1S) we determined the fraction of long-lived μp(2S) to be $\sim 1.5\%$ for pressures between 1 and 64 hPa. Another analysis involving μp(1S) with a kinetic energy of ~ 1 keV originating from quenching of thermalized μp(2S) via the resonant process $\mu p(2S) + H_2 \rightarrow \{[(pp\mu)^+]^* pee\}^* \rightarrow \mu p(1S) + p + \ldots + 2$ keV gives the same result. This is the first direct observation of long-lived μp(2S) atoms.

We are preparing a measurement of the $2S$ Lamb shift in muonic hydrogen, which will improve the uncertainty on the RMS proton charge radius by more than one order of magnitude. Technical aspects of our experiment are presented, including a new low-energy negative muon beam, an efficient low-energy muon entrance detector, a randomly triggered 3-stage laser system providing 0.5 mJ, 7 ns laser pulses at 6.02 μm wavelength, and a large solid angle xenon gas-proportional-scintillation-chamber (GPSC) read out by a microstrip-gas-chamber (MSGC) with a CsI-coated surface for the detection of 2 keV X-rays.

1 Introduction

Hydrogen-like atoms have served extensively as very successful probes of the basic aspects of the laws of physics. It is the detailed investigation of the hydrogen atom that led to the development of quantum mechanics and it is the discovery of the Lamb shift in 1947 [1] that motivated the description of physical processes via quantum field theory. Clearly, it is by further precision measurements that unexpected features of physical law can be discovered.

⋆ email: Randolf.Pohl@psi.ch

Optical spectroscopy of electronic hydrogen has improved tremendously over the past few years and now reached a point where the proton size affects the interpretation of the results [2,3,4]. The present knowledge of the charge radius, however, is not very precise. It stems mainly from the traditional method for obtaining nuclear radii, electron scattering [5,6,7,8,9]. However, because the proton radius is very small and hydrogen targets have low density and must be contained within a vessel, the experiments are quite difficult to perform and to analyze. The analysis converts the shape of the momentum-transfer dependent scattering cross section into an rms radius. There are, as pointed out recently [10], normalization problems. These problems lead to inconsistent results as can be seen from Fig. 1.

To overcome this limitation will require the measurement of the Lamb shift (the $2S$-$2P$ energy difference) in muonic hydrogen. Here the main QED contribution is vacuum polarization, for which calculations are now available at a precision level of 10^{-6} [11,12,13,14]. Because the effect of the finite proton size contributes as much as 2% to the μp Lamb shift, a precise measurement of the shift will provide an accurate value of the proton radius. The knowledge of the proton radius has intrinsic interest as a fundamental quantity, and is important in other measurements. A measurement of r_p at 0.1% precision will permit QED calculations of bound systems to be compared with the ep experiments at a precision level of few$\times 10^{-7}$ gaining an order of magnitude over the present limits.

We are setting up an experiment to measure the energy difference $\Delta E(2\,^3S_{1/2} - 2\,^5P_{3/2})$ in a laser resonance experiment to a precision of 30 ppm, which corresponds to 10% of the natural linewidth, to deduce the proton radius with 10^{-3} relative accuracy, 20 times more precise than presently known. An important pre-

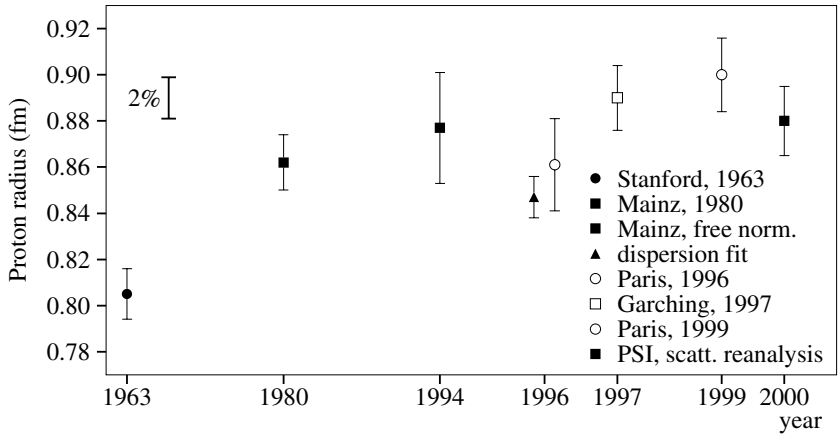

Fig. 1. The different values for the rms charge radius of the proton as obtained from electron scattering experiments (full symbols) and hydrogen spectroscopy (open symbols)

requisite to this experiment is the availability of long-lived ($\sim 1\mu$s) metastable μp(2S). This has been investigated in detail during recent years at PSI. Advances in muon beam quality, laser technology, and low-energy X-ray detectors have come to the point where the measurement of the Lamb shift in muonic hydrogen is possible.

In this paper we first give an overview of our experiments on the population of long-lived μp(2S) achievable by stopping muons in a hydrogen gas target at a few hPa pressure. The second part describes the experimental setup of the laser experiment which will go into operation in the year 2001.

2 Long-Lived Metastable μp(2S)

A number of experiments have been performed investigate the formation of long-lived metastable μp(2S) when muons are stopped in low-pressure hydrogen target gas. X-ray measurements [15,16,17] have shown that, depending on the hydrogen gas pressure, around 4% of the muons reach the 2S state. Collisional quenching, however, may deexcite these μp(2S) in an interaction with a molecule of the surrounding hydrogen gas:

$$\mu p(2S) + \mathrm{H}_2 \rightarrow \mu p(2P) + \mathrm{H}_2 \rightarrow \mu p(1S) + \mathrm{H}_2 + \mathrm{K}_\alpha \; . \tag{1}$$

At a kinetic energy below 0.31 eV, which is the μp(2S) $\rightarrow$ μp(2P) threshold energy in the laboratory frame, the above quenching reaction of the μp(2S) state is energetically forbidden. So, the previously accepted scenario was, that μp(2S) atoms formed at kinetic energies below this quenching threshold should be long-lived (i.e. with a lifetime of O(1 μs)) because the quenching should only take place via Stark mixing

$$\mu p(2S) + \mathrm{H}_2 \rightarrow \{\mu p(\alpha\,|2S\rangle + \beta\,|2P\rangle) + \mathrm{H}_2\} \begin{array}{l} \nearrow\ \mu p(2S) + \mathrm{H}_2 \\ \searrow\ \mu p(1S) + \mathrm{H}_2 + \mathrm{K}_\alpha \end{array} \tag{2}$$

during the collision time of $\sim 10^{-14}$ s. Since the radiative rate of the 2P level is $\sim 10^{11}\,\mathrm{s}^{-1}$ the μp(2S) atom should undergo of the order of a thousand collisions before radiative decay via Stark mixing should take place. This would result in a lifetime of the 2S state of the order of one microsecond at a few hPa H_2 pressure.

Moreover, also the μp(2S) atoms formed at a kinetic energy above 0.31 eV should contribute to the final long-lived μp(2S) population as they can be slowed down to below threshold before they are quenched. Theoretical considerations [18,19] show, that up to a few eV the cross sections for quenching according to (1) and the one for slowing down are of the same order of magnitude. Thus, a μp(2S) formed at a kinetic energy above the quenching threshold has an appreciable probability to slow down without being quenched (the so-called μp(2S) "survival probability") thereby increasing the final number of long-lived μp(2S).

2.1 Measurement of the Initial Kinetic Energies of μp(1S) Atoms

To determine the initial kinetic energy distributions of muonic hydrogen atoms we stopped low energy muons along the axis of a cylindrical low pressure gas target, and detected the time difference between the muon stop and the arrival of the μp atom at the inner gold-coated surface of the cylinder. The target was located in a strong axial magnetic field which forced the muons to follow the field lines but did not affect the neutral μp system.

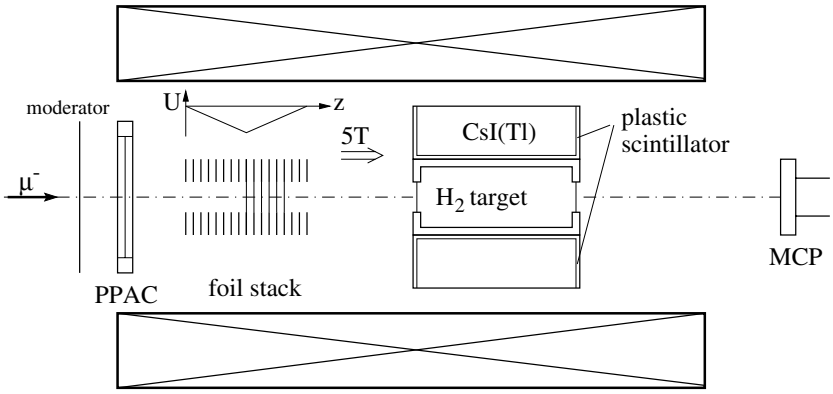

Fig. 2. Experimental setup for the kinetic energy experiment. The PSC solenoid provides an axial magnetic field of 5 Tesla. PPAC: Parallel plate avalanche chamber. MCP: Microchannel plate. The photomultipliers and light-guides coupled to the CsI and plastic scintillators are not shown

The experimental setup is shown in Fig. 2. Muons at 10 MeV/c from the πE5 beam channel at PSI enter the PSC solenoid. At the exit of the parallel plate avalanche chamber (PPAC) the muons have energies between 0 and 200 keV and the beam diameter is a few mm. The 5 Tesla magnetic field limits the cyclotron radii to about 1 mm. The muons cross a stack of thin carbon foils (5 μg/cm^2) where a few electrons are released. Since the carbon foils are kept at negative high voltage, the electrons from the foil are accelerated, traverse the gas target (following the magnetic field lines) and are detected by a microchannel plate (MCP). The foil stack acts simultaneously as a detector for keV muons and reduces the phase space volume of the beam by frictional cooling [20].

The gas target consists of an Al cylinder with 58 mm inner diameter and two thin (2 μg/cm^2) Formvar foil windows supported by grids. The inner cylinder wall is coated with a vacuum-deposited gold layer. When a μp atom reaches the wall the muon is transferred to gold and μAu X-rays of MeV energies are emitted. The μAu X-rays (2 to 9 MeV) are detected by a large CsI crystal which surrounds the target. The measured μAu time-of-flight (TOF) spectrum gives precise information on the μp kinetic energy distribution. To extend our sensitivity to the kinetic energies between thermal energy and a few hundred eV

we used various target diameters between 7 mm and 58 mm diameter. Smaller targets are more sensitive to smaller kinetic energies, and the use of different target diameters is also a very strong consistency check of our method.

The measured time spectra were then fitted using Monte Carlo generated time spectra for a grid of ~ 65 kinetic energies between thermal energy and a few hundred eV.

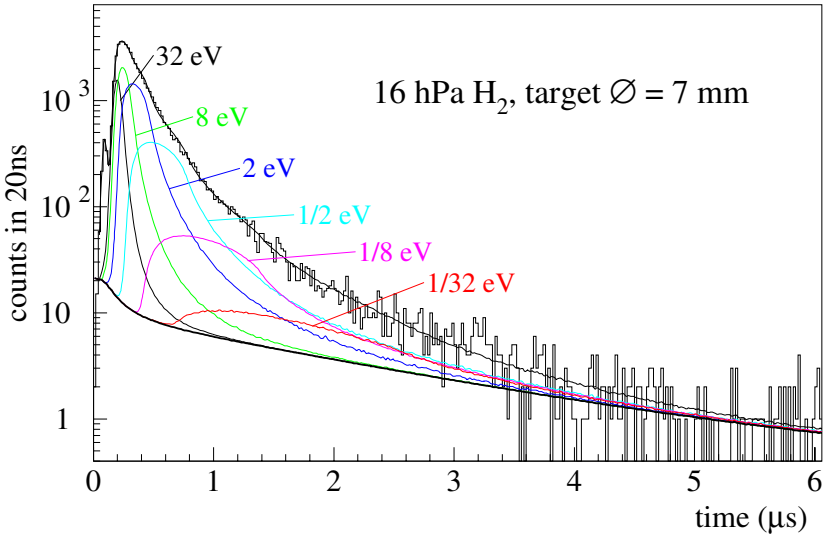

Fig. 3. Time distribution of μAu x rays measured with the 7 mm target at 16 hPa H_2 pressure. For better clarity the fit is a superposition of only 6 time spectra with single μp energies $E_{\rm kin} = 1/32$, 1/8, 1/2, 2, 8, 32 eV. To obtain the final result we used a much finer grid of kinetic energies

The Monte Carlo code includes the effect of elastic scattering of muonic hydrogen on hydrogen molecules [21,22] as well as backscattering of muonic hydrogen atoms from the gold layer of the target chamber walls. An example of a measured spectrum at 16 hPa and the function fitted to the data (only a reduced set of 6 functions is used here for illustrative purposes) can be seen in Fig. 3. Figure 4 shows the initial kinetic energy distribution obtained at this pressure using the full set of MC generated functions.

It has to be stated, however, that this experiment determines the initial kinetic energy distribution of μp(1S) atoms, since the μp(2S) atoms are quickly thermalized and do not reach the target chamber walls. However, a cascade code, which is also able to reproduce the measured K-yields and initial kinetic energies at all hydrogen gas densities under consideration shows that the initial kinetic energy distribution of the μp(2S) atoms differs negligibly from the one of μp(1S). This is not surprising, because at pressures in the few tens of hPa region

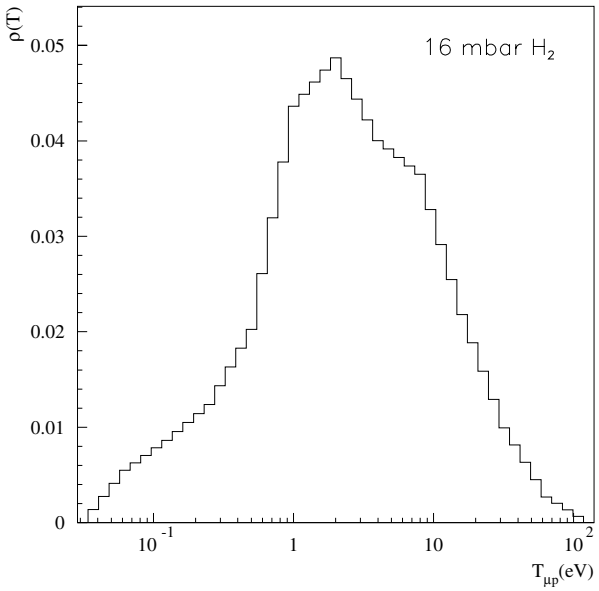

Fig. 4. Initial kinetic energy distribution measured at 16 hPa H_2 gas pressure. One can see the appreciable fraction of μp atoms formed at kinetic energies below 0.31 eV

the cascade processes are predominantly radiative for $n < 9$, and at higher n-values — where $E_{\rm kin}$ can be changed — collisional Stark mixing of the ℓ-states dominates all other processes and thus smears out possible differences in the "cascade history" of μp(1S) and μp(2S) atoms.

Taking the fact that at 16 hPa 4% of all muons reach the 2S state and assuming a conservative number for the slowing down probability of μp(2S) initially formed at energies above 0.31 eV, we can give a preliminary number of $\sim 1.5\%$ for the fraction of metastable μp(2S) per muon stopped in hydrogen.

2.2 Direct Observation of Resonantly Quenched 2*S* States

Earlier experiments [15,17,23] aiming to observe delayed Lyman-α X-rays following radiative quenching of thermalized μp(2S) atoms (Eq. 2) had not found any delayed events. Thus, they seemed to give rather low upper limits for the long-lived metastable μp(2S) population under the assumption that the main decay channel of thermalized μp(2S) atoms is radiative quenching.

This apparent contradiction between our results from the kinetic energy measurement and the earlier experiments prompted us to perform another analysis of our TOF data set. Following a suggestion made by P. Froelich and A. Flores-Riveros [24] we looked for high-energetic ($\sim$ 1 keV) μp(1S) atoms produced by

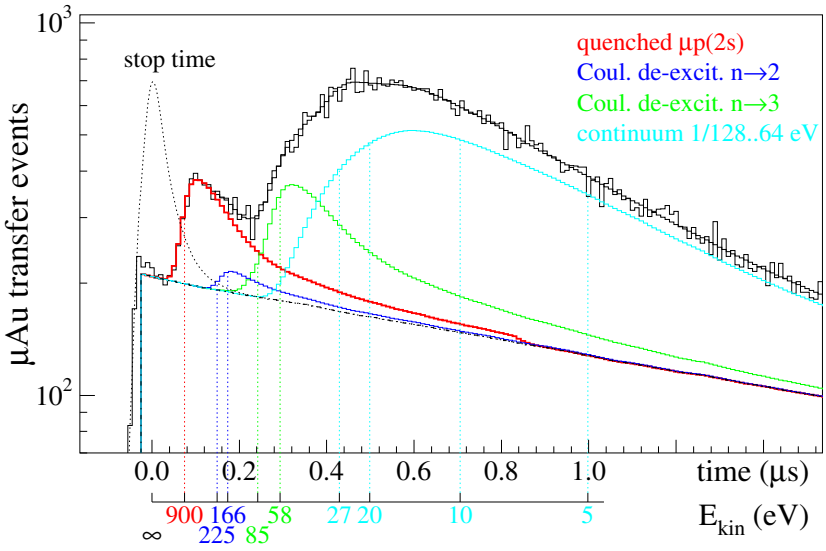

Fig. 5. Early part of the TOF spectra taken at 64 hPa H_2 pressure in the 58 mm diameter target, together with a fit of the spectra. The thick, red function corresponds to the resonantly quenched μp(2S) resulting in a 900 eV kinetic energy component convoluted with a (fitted) 2S lifetime. The fit function also includes a "continuum" as seen in the previous figure, plus some extra energies which make up the so-called "Coulomb deexcitation" part. The dashed peak indicates the measured stop time distribution. The measured background and a kinetic energy scale corresponding to the TOF are also shown

resonant molecule formation from the 2S-state and subsequent autodissociation

$$\mu p(2S) + H_2 \rightarrow \{[(pp\mu)^+]^* pee\}^* \rightarrow \mu p(1S) + p + \ldots + 2\,\mathrm{keV} \qquad (3)$$

In this process, which has been discussed by several authors [25,26,27,28,29], the 2S–1S energy difference of $\sim$ 2 keV is shared among the μp(1S) and one proton. This results in μp(1S) atoms with a kinetic energy of $\sim$ 900 eV (see Fig. 5).

Figure 6 shows the early part of the TOF spectra taken at pressures between 64 and 4 hPa, using our largest diameter target (58 mm). One sees a pressure-dependent lifetime of the 900 eV component which proves that this component stems from long-lived μp(2S) diffusing around in the H_2 target gas until they eventually undergo reaction (3). If the $n = 2 \rightarrow 1$ transition took place during the initial cascade, i.e. without long-lived μp(2S), the decay time of the 900 eV component would not change with pressure, but would rather be determined by the geometry of the target alone (which was the same for all measurements shown in Fig. 6). After a more detailed analysis we will give a precise number for the long-lived μp(2S) population, the lifetime of the 2S state and the cross section for process (3).

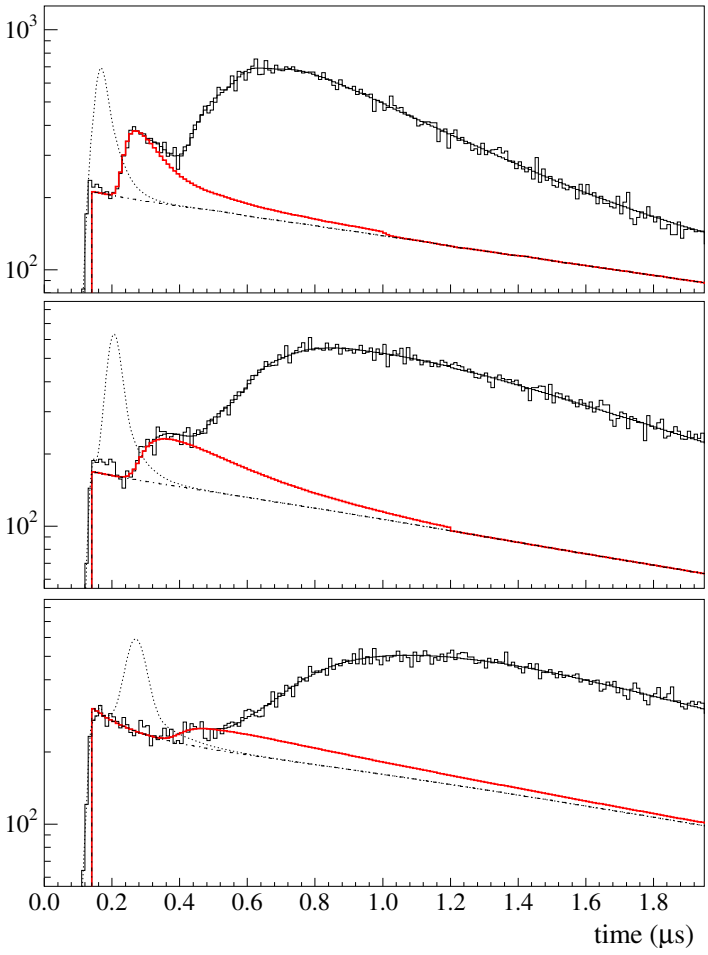

Fig. 6. Early part of the TOF spectra taken at 64, 16, and 4 hPa (top, middle, bottom, respectively) in the 58 mm diameter target. (The fitted functions were obtained by simultaneously fitting the data taken at two target diameters (20 and 58 mm) at each pressure). One can clearly observe a change in the lifetime of the high-energetic ($\sim$ 900 eV) component (thick red curve), which shows that this component is produced when the thermalized $\mu p(2S)$ are quenched. The dashed peak indicates the measured stop time distribution. The background is also shown

3 Laser Experiment

With the ability to produce a sufficiently large number of long-lived $\mu p(2S)$ atoms in a very small volume (a few cm^3 at a few hPa pressure) we have now come to the point where a laser resonance experiment to measure the Lamb shift of muonic hydrogen is possible. Such an experiment is under preparation and will start data taking in 2001. The experimental setup consists of three major

parts which will be described here, namely the high-intensity low-energy muon beam line, the three-stage laser system for 6 μm light, and the low-energy X-ray detectors to observe the laser-induced 2 keV X-rays from the $\mu p(2P \rightarrow 1S)$ transition following the laser excitation $\mu p(2S \rightarrow 2P)$.

3.1 High-Intensity Low-Energy Muon Beam Line

In order to obtain a sufficiently high muon stop rate inside a low density target gas a new high-intensity low-energy muon beam line has been built at PSI (Fig. 7). Negative pions with 100 MeV/c momentum are injected into the Cyclotron Trap [30], where they traverse a radial moderator which brings them to a suitable orbit in the Trap. They decay into muons which are slowed down from MeV to keV kinetic energies by a set of thin Formvar foils placed in the center of the Trap. An axial electric field ejects the muons along the Cyclotron Trap axis and out of the Trap field region (up to 4 Tesla) after they have been slowed down to kinetic energies around 20 keV. This method of producing low-energy muons was successfully tested [31]. The rate of keV-muons is enhanced by more than an order of magnitude relative to a conventional cloud muon beam.

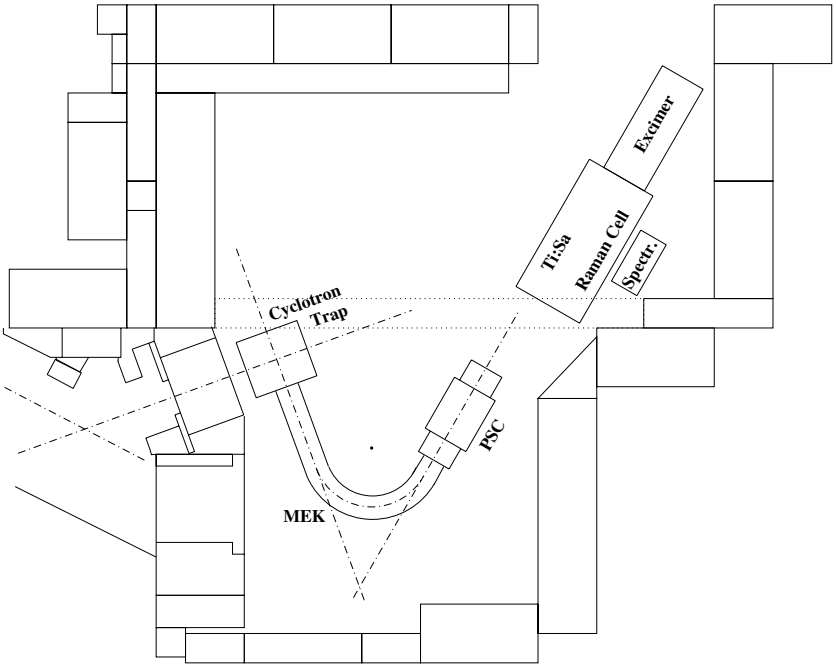

Fig. 7. Lay-out of the πE5 area with Cyclotron Trap, magnetic channel MEK, PSC solenoid, and laser components

Following the Cyclotron Trap the curved magnetic Muon Extraction Channel (MEK), operated at 0.15 T, transports the muons from a region of high neutron background (near the pion beam exit and the Cyclotron Trap) to the PSC solenoid where the laser resonance experiment is performed. It simultaneously acts as a cleaning filter because particles with momenta above ~ 4 MeV/c are not transported through the curvature while about 90% of the good muons (typically 20 keV energy, 2 MeV/c momentum) are transported from the Trap to the solenoid. The muon trajectories make a vertical drift (relative to the magnetic field lines) of ~ 2 cm, proportional to the particle momentum. This separates muons from the high flux of keV electrons which have almost negligible vertical drifts.

Finally the muons enter the PSC apparatus. Lead collimators at the PSC entrance (not shown in the figure) define a 15 mm wide and 5 mm high muon beam at energies between 10 and 40 keV. Two foil stacks inside the PSC of the type as used in our previous experiment described above act as detectors for slow muons (dE/dx near the Bragg peak) and reduce the width of the kinetic energy distribution. The stack detectors have time resolutions of better than 5 ns, to be compared with the muon time-of-flight (TOF) between the two stacks of typically 150 ns. A trigger for the laser will be given by a muon detected in both detectors with the correct TOF.

The muon rate can be predicted from test measurements [31] to reach about 100 $\mu^-/(\mathrm{cm}^2 \cdot \mathrm{keV} \cdot \mathrm{mA} \cdot \mathrm{s})$ in the PSC solenoid, corresponding to about 600 muon stops per second in a 10 hPa H_2 target, 15 cm long, for a beam size 5×15 mm^2.

3.2 Three-Stage Laser System for 6 μm Light

Our laser system consists of three stages: A XeCl excimer laser, a combination of dye and Ti:Sa laser, and a H_2 Raman cell for conversion to 6 μm (Fig. 8).

When a randomly incoming muon is detected by the foil stack inside the solenoid, the laser is triggered. Because of the short muon lifetime the laser light has to arrive in the target within less than $\sim$1 μs. For this reason our first stage of the laser system consists of a 50 Hz XeCl excimer laser delivering 28 ns long pulses of 600 mJ at 308 nm. The delay caused by the excimer laser is only about 300 ns from trigger to laser pulse.

The second stage, conversion of the 308 nm light from the excimer laser to the 708 nm light needed as input of the Raman shifter, is done in two substeps. The 308 nm light pumps a dye cell, which delivers the $\sim$500 nm light required to pump the Ti:Sa laser. The conversion in two steps from 308 nm to 708 nm is also favorable because in contrast to a simple dye cell the cavity-dumped Ti:Sa laser produces a short pulse ($\sim$7 ns) with TEM_{00} profile. A good beam quality at 708 nm is required since the Raman cell only shifts the wavelength of the Gaussian part of the incoming radiation.

In the third stage the 708 nm light is converted to 6.02 μm via third Stokes Raman shift in a high pressure hydrogen cell. The 0.5 mJ, 7 ns long pulses are injected into a multipass cavity inside the gas target in order to effectively illuminate the muon stop region.

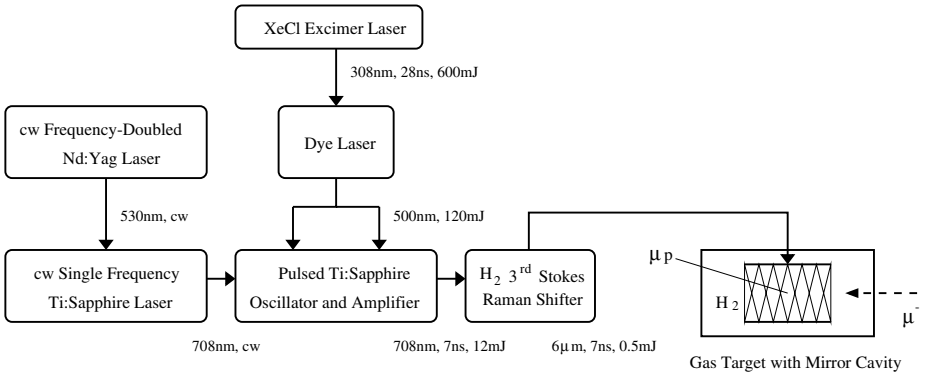

Fig. 8. The components of the laser system. The high power XeCl excimer laser pulse triggered my the muon entrance detector is converted in two steps to a high quality 7 ns long pulse of 708 nm which is shifted to the desired 6 μm light inside the multipass Raman cell. The light is injected into a multipass cavity to effectively illuminate the muon stop volume inside the PSC solenoid. High resolution frequency selection is provided by injection of a cw Ti:Sa laser

3.3 X-Ray Detector

The 2 keV X-ray detector will consist of two 20×6 cm^2 xenon gas-proportional-scintillation-chambers (GPSC) as were used in previous experiments [32,33]. These chambers produce a secondary scintillation light at 170 nm which leads to large amplitude pulses with low statistical fluctuations. GPSCs combine large detection areas with good energy resolution and almost linear energy response. These detectors are insensitive to magnetic field.

Recent developments of the collaborators from Coimbra [34,35] permit the detection of the secondary scintillation light using a Microstrip Gas Chamber (MSGC). The UV photons are detected by CsI-coated thin-film photocathodes deposited directly onto a microstrip plate (MSP). A system has been developed where a thin quartz window separates the xenon GPSC from the MSGC, filled with P10 (Ar + 10% CH_4) gas or xenon gas. A schematic view of the operation is shown in Fig. 9.

4 Conclusions

We have for the first time observed long-lived $\mu p(2S)$ atoms. The analysis gives a population of $\sim 1.5\,\%$. Another, independent analysis, using the low-energy part of the initial kinetic energy distribution and relying on the calculated "survival probability" for $\mu p(2S)$ atoms formed at kinetic energies around 1 eV, gives the same result.

Experiments in optical spectroscopy of electronic hydrogen have come to the point where a precise value of the proton radius is urgently needed for the interpretation of the results. Laser technology and X-ray detection schemes have

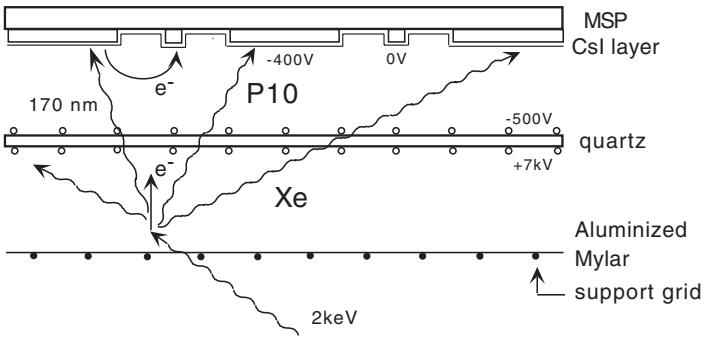

Fig. 9. Schematic view of the operation of a MSGC based GPSC. X-rays of a few keV are converted into primary electrons which drift toward the GPSC anodes located on the quartz. The electrons produce secondary scintillation light proportional to the energy of the X-ray. The secondary photons cause photoelectrons emission in the CsI coated MSGC cathode. The electrons are multiplied near the anode to give the signal

developed rapidly in recent years and are used routinely nowadays, and long-lived metastable $\mu p(2S)$ can for the first time be created in a sufficiently large number inside a small stopping volume.

We now have the opportunity to perform a laser resonance experiment to measure the Lamb shift in muonic hydrogen. Taking into account the muon stop rate, entrance detector efficiency, long-lived metastable 2S population, laser transition probability, solid angles and detection efficiency of the X-ray detector we estimate our event rate on resonance to be 9 events per hour.

A precision of 30 ppm for the Lamb shift in muonic hydrogen, i.e. an uncertainty on the proton radius of 10^{-3}, can therefore be achieved within a reasonably short measuring time. Better accuracy of the proton radius will then be limited by effects of proton polarizability [36,13].

Acknowledgments

We would like to thank A. Adamczak for providing us with the detailed tables of cross sections, final energies and scattering angles for the scattering of $\mu p(1S)$ on hydrogen molecules, which are used in our Monte Carlo code. J.S. Cohen and V.S. Melezhik provided us with their new results on the differential scattering cross sections of $\mu p(1S)$ on hydrogen at kinetic energies as high as 1 keV. R. Rosenfelder has stimulated our work via fruitul discussions.

References

1. W. E. Lamb, Jr. and R. C. Retherford: Phys. Rev. **72**, 241 (1947)

2. S. Bourzeix et al.: Phys. Rev. Lett. **76**, 384 (1996)
3. Th. Udem et al.: Phys. Rev. Lett. **79**, 2646 (1998)
4. C. Schwob et al.: Phys. Rev. Lett. **82**, 4960 (1999)
5. L.N. Hand: Rev. Mod. Phys. **35**, 335 (1963)
6. G.G. Simon et al.: Nucl. Phys. **A 333**, 381 (1980)
7. C.W. Wong: Int. J. Mod. Phys. **3**, 821 (1994)
8. P. Mergell et al.: Nucl. Phys. **A 596**, 367 (1996)
9. R. Rosenfelder: Phys. Lett. **B 479**, 318 (2000)
10. S. G. Karshenboim: Can. J. Phys. **77**, 241 (1999)
11. K. Pachucki: Phys. Rev. **A 53**, 2092 (1996)
12. T. Kinoshita and M. Nio: Phys. Rev. Lett. **82**, 3240 (1999)
13. K. Pachucki: Phys. Rev. **A 60**, 3593 (1999)
14. J.L. Friar et al.: Phys. Rev. **A 59**, 4061 (1999)
15. H. Anderhub et al.: Phys. Lett. **71 B**, 443 (1977)
16. H. Anderhub et al.: Phys. Lett. **143 B**, 65 (1984)
17. P.O. Egan et al.: Phys. Rev. **A 23**, 1152 (1981)
18. G. Carboni and G. Fiorentini: Nuov. Cim. **39 B**, 281 (1977)
19. T. Jensen and V. Markushin: PSI-PR-99-32, nucl-th/0001009
20. M. Mühlbauer et al.: Hyperfine Interact. **119**, 305 (1999)
21. A. Adamczak et al.: At. Data and Nucl. Data Tables **62**, 255 (1996)
22. J.S. Cohen: Phys. Rev. **A 43**, 4668 (1991) and private communication
23. J. Böcklin: PhD thesis ETH 7161 (1982), unpublished
24. P.Froelich and A.Flores-Riveros: Phys. Rev. Lett. **70**, 1595 (1993)
25. S.Hara, T.Ishihara: Phys. Rev. **A 40**, 4232 (1989)
26. I.Shimamura: Phys. Rev. **A 40**, 4863 (1989)
27. P.Froelich, J.Wallenius: Phys. Rev. Lett. **75**, 2108 (1995)
28. J.Wallenius, P.Froelich: Phys. Rev. **A 54**, 1171 (1996)
29. S.Jonsell, J.Wallenius, P.Froelich: Phys. Rev. **A 59**, 3440 (1999)
30. PSI, Annual Report, *General Volume*, 32 (1997)
31. P. de Cecco et al.: Nucl. Instrum. Methods **A 394**, 287 (1997)
32. J. Böcklin et al.: Nucl. Instrum. Methods **176**, 105 (1980)
33. H. P. von Arb et al.: Nucl. Instrum. Methods **207**, 429 (1983)
34. J.F.C.A. Veloso and J.M.F. dos Santos, and C.A.N. Conde: Nucl. Instrum. Methods **A 422**, 273 (1999)
35. J.F.C.A. Veloso and J.M.F. dos Santos, and C.A.N. Conde: IEEE Trans. Nucl. Sci. **44**, 73 (1997)
36. R. Rosenfelder: Phys. Lett. **B 463**, 317 (1999)